

# Impacts of Leading Edge Pitting and Delamination on Aerodynamic Characteristics of Wind Turbine Blades under Shear Inflow

Yan WANG\*, Yongfen CHAI, Chenglin DUAN, Jian ZHENG

**Abstract:** Undesirable performance degradation occurs when wind turbine operates in harsh environment, thus investigation of the impact of various degrees of leading edge erosion on the aerodynamic characteristics of wind turbine is significant and highly desirable. In this study, significant research efforts were made to explore the effects of leading edge pitting and delamination on blade surface streamlines, flow structures, pressure coefficients, and aerodynamic forces of horizontal wind turbine under shear inflow. The  $k-\omega$  shear-stress transport turbulence model was adopted to close the three-dimensional incompressible Reynolds-averaged Navier-Stokes. The results indicate the existence of significant differences on surface streamlines between the smooth and eroded blade. The leading edge of the entire blade gets covered with the attached flow, while just a small area for the eroded blade is covered when it is at the lowest position. Moreover, small separation bubble appears at the suction surface of the section near the blade root, which grows bigger and induces a second vortex when the section moves to the middle of the blade and then the size gets smaller when the section is near the blade tip. With the increase of erosion, the pressure difference of blade surface decreases, indicating a severe decrease in performance of eroded blade. Furthermore, leading edge erosion causes a decrease in average torque coefficients by 19.75, 29.01, 41.82, and 42.54% for various leading edge erosion cases at the inflow wind speed of  $10 \text{ ms}^{-1}$ , and 25.0, 49.6, 51.3, and 54.6% at the speed of  $20 \text{ ms}^{-1}$ .

**Keywords:** aerodynamic characteristics; pitting and delamination; shear inflow; wind turbine blade

## 1 INTRODUCTION

Wind energy has developed rapidly during the past twenty years. By 2020, the global cumulative wind power capacity has reached up to 753 GW, which is further expected to increase in the next few years [1, 2]. Based on the requirements of more wind energy conversion together with site resources constraints, modern wind industry may face the challenges associated with development of larger-scale wind turbines and operation in harsh environments [3, 4]. It has been reported that larger-size modern wind turbines with higher tip speeds when operated in harsh climates are sensitive to leading edge erosion of wind turbine blade, which is a serious concern in wind industry [5]. However, still there is a continuous tendency to increase hub height and rotor diameter for optimizing the energy cost [6]. At present, the average hub height of wind turbine installed in the USA is 90 m and the rotor diameter is 121 m, both exhibiting significant increase from the comparable sizes of 82 m and 102 m, respectively, in 2015 [7]. In Europe, the wind turbine is typically larger and the average power capacity of installed wind turbine is 7.8 MW with rotor diameter greater than 140 m [6]. With the successful installation of GE Haliade-X 12 MW in Netherlands, the diameter and hub height of the wind turbine have reached 220 m and 260 m, respectively. In China, the greatest installed wind turbine has a rated power capacity of 10 MW with a rotor diameter of 185 m. The blade with significantly large size and high tip speed gets easily impacted by the inflow conditions and eroded by various types of environmental and tribological effects [4].

Wind shear, the change in wind speed with height, is one of the important sources of torque fluctuation, output power fluctuation, and aerodynamic loadings and rotor fatigue loads of wind turbine [8]. Wind shear is always caused by several common atmospheric phenomena, such as surface friction, land topography, low-level jets, and outflow from thunderstorms [9, 10]. The impacts of wind shear on turbine power generation have been extensively researched. Shear can decrease the power coefficient for megawatt turbines, and the diurnal variations of wind shear also lead to corresponding diurnal variations in power

production. It was found that the power output of a theoretical wind farm could increase by about 0.5% and decrease by 3% when the wind shear was considered [11-13]. Murphy et al. [14] explored the impact of wind shear on actual power generation of a megawatt-scale wind turbine operated in North America. The results demonstrated that the high wind shear could lead to a 5 and 4% higher than rated increase of power production, and low shear caused a reduction of power production by 1.7 and 2% in different cases. Rebecca et al. [6] reported that the frequency of high shear exponents ( $\alpha > 0.2$ ) appeared to be more (48%) than that (12%) of low shear exponents ( $\alpha < 0.2$ ). Fadaeinedjad et al. [15] showed that wind shear could induce  $3p$  frequency periodic impacts on power output of a wind turbine. Moreover, a lot of simulation-based studies qualified the effects of shear and shear-based direction or velocity on the power magnitude. Wagner et al. [16] pointed out that the shear of inflow in speed was more influential than directional veer on the power production. Therefore, significant research attention is required toward the shear influence on the wind turbine aerodynamics.

Erosion on the leading edge of turbine blade is also a dominant problem encountered by wind industry [17, 18]. It has been found that leading edge erosion occurs only after 2 years of operation of a wind mill, much earlier than the expected service age [4]. The erosion may start with small shallow pits near the leading edge; then it grows in depth, size, and density as the turbine operates; and gradually merges into surface gouges. If the maintenance is not carried out in time, the gouges combine to delamination [19, 20]. The Offshore Wind Innovation Hub [21] pointed out that leading edge erosion is the urgent blades affair for all wind industry operators and manufacturers. In 2018 [5], an emergency blade repair of 140 out of 175 turbines in the 630 MW wind farm was performed only after one month of installation. The above-mentioned studies indicate that leading edge erosion of the blade is a prominent issue for wind power industry that should be appropriately addressed urgently.

Blades are the important parts of wind turbine to absorb and convert wind energy, which affects the operation, management, and maintenance of the wind

farm. The erosion level of a blade is decided by the air foil shape, rotating speed of tip, and operating environment, which make it difficult to determine the evolution of erosion with timeline, and the study on erosion effects always typically use given erosion stages and quantities. Powell [22] investigated the power loss of an unprotected 1.5 MW wind turbine through field experiment and found that it could reach up to 20-30% after five years of operation. Gaudern et al. [23] categorized the erosion stages of Vestas turbines that had been operated for about five years, and found that all levels of erosion degraded the aerodynamic coefficients of the airfoil, and even the “minimal erosion” pits of paint loss scattered at the surface of the leading edge could decrease/increase the lift/drag coefficients by 4%/49%, respectively. Sareen et al. [20] experimentally studied various leading edge erosions at the range of 10% $c$  to 13% $c$  of the DU96-W-180 airfoil and found that leading edge erosion could increase the drag by 6-500%, and resulted in a reduction in the annual energy production (AEP) of the turbine by about 5-25%, where  $c$  is the chord length. Gharali and Johnson [24] found that various leading edge defect lengths and thicknesses could cause a lift decrease by 17-76% for S809. Further, Ge et al. [18] explored the surface concaved deep defects and surface distributed shallow defects on the aerodynamic characteristics of S809, and found that the maximum lift coefficient of the eroded airfoil dramatically decreased by 35 to 61% and the drag coefficient notably increased by 131 to 217%. Han et al. [25] quantitatively analyzed the influences of different levels of erosion on the aerodynamic forces of NACA 64-618 airfoil. The results demonstrated that leading edge erosion could induce a lift decrease by 53% accompanied by a drag increase by 314%, resulting in a 2 to 3.7% AEP loss for 5 MW NREL turbine. Wang et al. [26, 27] investigated the effects of pits and defects on the aerodynamic performance of S809, and results indicated that the maximum lift reduction could reach up to 36%, and when the ratio of defect length to thickness was greater than 0.5, the aerodynamic performance was mainly determined by the erosion thickness.

It can be concluded that leading edge erosion of turbine blade has attracted tremendous research interest and concerns worldwide, and significant insights into the effects of erosion have been obtained. However, some problems and challenging issues are still encountered which undeniably need further systematic explorations: (i) most researches have focused on two-dimensional (2D) airfoils, for example, Wang et al. [26, 27], Ge et al. [18], Sareen et al. [22], and Gharali and Johnson [24] mainly paid attention to the effects of pits, defects, gouges, and delamination at the leading edge of airfoil. However, study about the impacts of leading edge erosion on the aerodynamic and flow characteristics of the wind turbine with 3D model is still lacking. In particular, comprehensive understanding and prediction on the impacts of blade leading edge erosion are not only conducive to the optimal design and maintenance of blade, but also beneficial for the operation and management of wind farm; (ii) some researchers such as Han et al. [25] and Francesco et al. [17] qualified the effects of erosion on the AEP of the wind turbine, but results were always obtained with Blade Element Method (BEM) theory and by using the GH Bladed or FAST. However, a deep elaboration on the influence mechanism and flow structure around the blade still lacks; (iii) due to the growth of physical dimensions of wind turbine, wind shear has been a significant influencing

factor for power generation. However, most studies related to leading edge erosion focused on uniform flow, and could not take wind shear into consideration. Studies on the aerodynamic characteristics of leading edge eroded wind turbine under shear inflow are still deficient.

To bridge the above-mentioned gaps, in this study, a systematic exploration was carried out on the leading edge eroded NREL Phase VI rotor under shear inflow. The pits and various sizes of delamination were distributed uniformly in the leading edge of the blade, and results were compared with those of the smooth blade. The main objective of this study is to provide a deep understanding of the impacts of leading edge erosion on the aerodynamic forces and flow structures of wind turbine blades, and the results present a valuable reference for the design and maintenance of blade. The results of this study are also very useful in the operation and management of the wind farm and in strategy-making for wind farm managements.

## 2 GEOMETRICAL MODEL AND NUMERICAL METHOD

### 2.1 Geometrical Model

The main objective of this study is to observe the impacts of leading edge pitting and delamination on the aerodynamic performance of wind turbine blades under shear inflow. Phase VI turbine designed and built by the National Renewable Energy Laboratory was selected for its detailed experimental data [28, 29]. This wind turbine is two-bladed with a diameter of 10.058 m, and the blade configuration was designed by using the S809 airfoil profile. The geometry and aerodynamic properties of the turbine model are well documented in the literature [28, 29]. For cases considered in current research, only the upwind rotor was examined, and no rotor cone angle and the blades were rigidly attached to the turbine hub. The rotor turns at a constant speed of 72 rpm. The blade pitch angle is set as 3° toward feather relative to the rotor plane.

**Table 1** The erosion parameters of the studied cases

Cases	Leading edge character
Smooth blade	no erosion
Erosion 1	Pits erosion, $h = 1 \text{ mm}$ , $x = 10\%c$
Erosion 2	Delamination, $h = 0.5 \text{ mm}$ , $x = 10\%c$
Erosion 3	Delamination, $h = 1 \text{ mm}$ , $x = 10\%c$
Erosion 4	Delamination, $h = 3 \text{ mm}$ , $x = 10\%c$

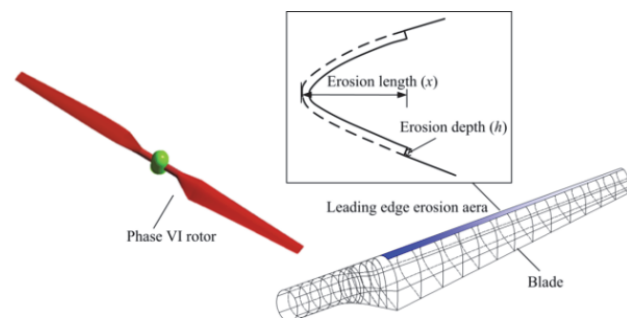


**Figure 1** Leading edge erosion configuration of Phase VI wind turbine

Literature reports have proven that the erosion of blade may cover the first 10% $c$  of a wind turbine blade and undergoes the following three stages: pits, gouges, and delamination [3, 4]. Owing to the difficulty in quantitative estimating the position and size of gouges on the surface of blade, only pits and three levels of delamination were

considered in current study and the erosion area was found to span uniformly over the first 10%*c* of the leading edge of the blade. The rotor configuration and the erosion schematic are shown in Fig. 1, and the erosion parameters are presented in Tab. 1, where *h* is the erosion depth, mm; and *x* is the erosion length, herein  $x = 10\%c$ .

**2.2 Computational Settings**

The computational field consists of a semi-cylinder and a cuboid, the radius of the semi-cylinder is 50 m (10*R*) and its length is 82 m (16*R*); the height of the cuboid is 12.2 m and *R* is the rotor radius. The wind turbine rotor is set at the height of 12.2 m above the ground, which is the same height as that in the wind tunnel experiments [29]. The rotor is placed at a distance of 21 m (about 4*R*) from the inlet, as shown in Fig. 2.

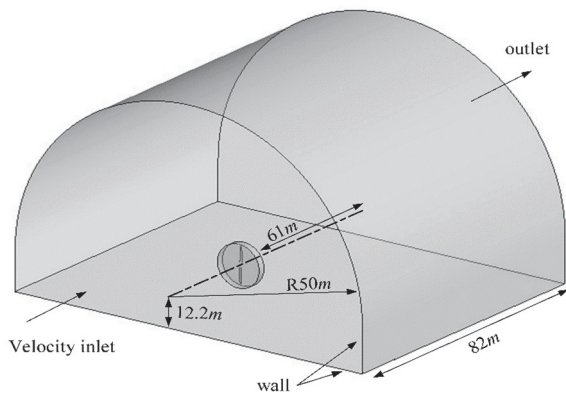


Figure 2 Computational field and boundary conditions

Hybrid meshes with structured, unstructured, and prism grids are generated in the computational domain. A 40-layers boundary layer is added for an accurate capture of the flow field structures on the blade surface; structured meshes are set in the boundary layer; and the first grid height is set as  $5 \times 10^{-5}$  m, which corresponds to  $y^+ = 1$ , so that the blade surface flow can be computed without using wall functions. In the rotating domain, 7 042 700 unstructured prism grids are arranged, and out of the rotating domain is the static area, where 3 949 900 structured grids are distributed.

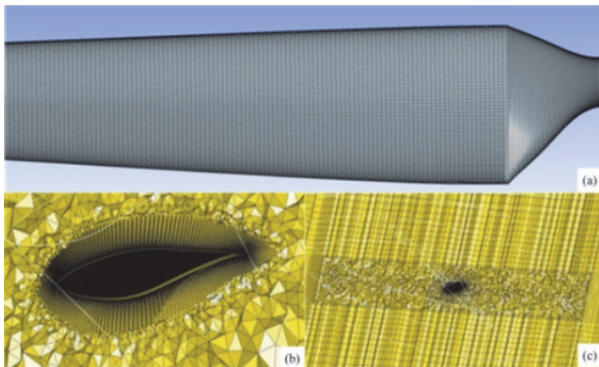


Figure 3 Local grids near the blade, in the boundary layer and rotating domain: a) grids near the blade surface; b) boundary layer grids; and c) the hybrid mesh in the rotating domain

The structured mesh in the boundary layer and the prism mesh in the rotation domain are shown in Fig. 3.

The computation was conducted using a small super computer, which has a 48-core CPU and a 256-DDR. The time to complete a simulation case was about one week, and a total of more than three months was taken for the present study.

**2.3 Turbulence Model**

Large eddy simulation (LES) and direct numerical simulation (DNS) are more accurate in capturing the details of flow field, and they are always used in fundamental research at low Reynolds number or small simulation domain. However, they may be expensive for practical engineering applications [28]. Compared with LES and DNS, Reynolds-averaged Navier-Stokes (RANS) is rather cheap, which is a useful tool in solving mean velocity field. To capture the complex flow characteristics and correctly predict the stall initiation, shear-stress transport (SST) *k- $\omega$*  turbulence model [30] was adopted throughout the study for its desirable results in the simulation of 2D separated flows and 3D turbine flow fields characteristics [27, 31]. In this study, ANSYS-Fluent was adopted to conduct the numerical simulations; and SIMPLE algorithm and segregated solver were used to solve the momentum and pressure equations. Second order scheme was adopted for discretization of turbulence energy, momentum, dissipative and convective terms, and below residual  $10^{-6}$  was set for convergence. Moreover, MRF rotating frame was used in the study.

**2.4 Boundary and Computational Conditions**

In the calculation, shear inflow and free flow boundary conditions were adopted for the inlet and outlet, respectively. Non-sliding wall surface was adopted for the blade surface and the ground, and sliding surface was used for the wind turbine surface. Interfacial boundary was adopted between the rotating and the static region. The shear wind at the inlet can be expressed in terms of Eq. (1) as follows:

$$v(z) = v_{hub} \left( \frac{z}{z_{hub}} \right)^\alpha \tag{1}$$

where  $v_{hub}$  is the average wind speed at the hub height, which can be inferred in Tab. 2;  $z_{hub}$  is the height of the wind turbine hub, herein  $z_{hub} = 12.2$  m; and  $\alpha$  is the wind shear coefficient, herein  $\alpha = 0.2$ .

Similar to the blind comparison test, only the upwind and non-yawed turbine configurations were used in current analysis. Wind speed was 10 and 20  $ms^{-1}$ .

**2.5 Numerical Validation**

Fig. 4 shows the simulation results of the pressure coefficients at the blade sections  $r/R = 0.3, 0.47, 0.63, 0.8,$  and  $0.95$ , respectively, where  $r$  is the position along the blade and  $R$  is the blade radius. The simulation is conducted at an average wind speed of 10  $ms^{-1}$ , and the results are compared with the experimental data [29]. In Fig. 4,  $x$  represents the calculation point in the chord direction of the blade and  $c$  is the chord length.

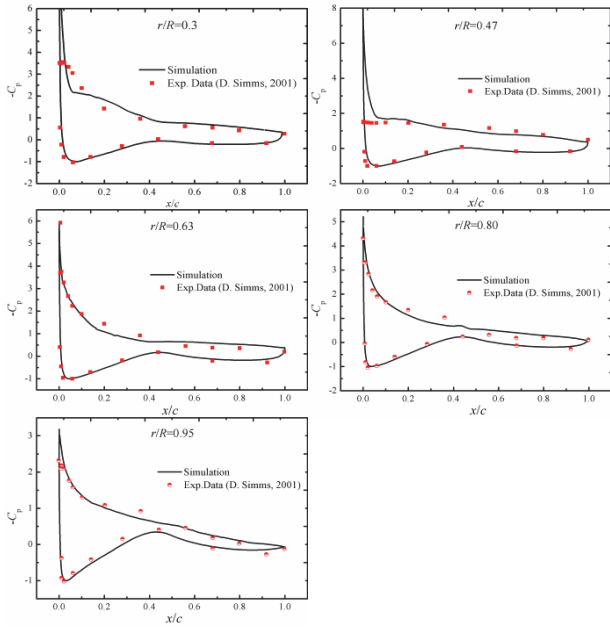


Figure 4 Simulated and experimental pressure distributions at 10 ms<sup>-1</sup>

The dimensionless pressure coefficient of the blade section can be calculated by using Eq. (2) as follows:

$$C_p = \frac{P - P_\infty}{\frac{1}{2} \rho (U_\infty^2 + (\omega r)^2)} \quad (2)$$

where  $P$  is the pressure of the blade section,  $P_\infty$  and  $U_\infty$  are the pressure and velocity of the inflow from infinity, respectively, and  $\omega$  is rotating speed of the wind rotor.

It shows that the pressure coefficient  $C_p$  calculated in this study in general exhibits a good accordance with those obtained from experiment. For section  $r/R = 0.3$ , the simulated  $C_p$  is basically consistent with the experimental result except a little underestimated at the 10% $c$  of the leading edge. For section  $r/R = 0.47$ , a simulation error of 10.2% is observed at 0.055 $c$  of the section, where the pressure is underestimated. This is mainly attributed to the large angle of attack and flow separation near the hub. The flow separation cannot be captured well, which leads to an underestimation of the pressure coefficient. At the section  $r/R = 0.63$ , the simulated  $C_p$  near the leading edge of the blade is completely consistent with the experiment data; however, an error of 15.6% can be observed at 0.2 $c$  of the blade suction surface. Similar results are also observed for the cross sections  $r/R = 0.8$  and  $r/R = 0.95$ . This is mainly due to the fact that the linear velocity and angle of attack at each cross section are different, and coupled with the 3D flow effects of the turbine, it results in simulation errors at the leading edge. However, in general, the deviations in the simulation are acceptable and the results obtained in this study can be used for further analysis.

### 3 RESULTS AND ANALYSIS

#### 3.1 Impacts on the Flow Characteristics Around the Blade

The analysis was conducted at the hub-height average wind speeds of 10 and 20 ms<sup>-1</sup>, respectively. The azimuth angle of the turbine rotor is shown in Fig. 5, when the turbine is rotating in counterclockwise direction.

Figs. 6 and 7 present the surface limiting streamlines of turbine blade at different azimuth angles. As the space is limited and pictures of the delaminated blade are similar, a case of Erosion 3 is selected to analyze the effects of leading edge erosion on the flow structure of the blade.

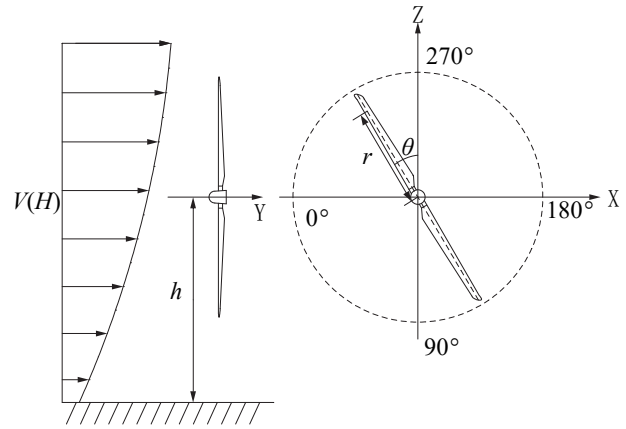


Figure 5 Illustration of wind turbine azimuth angle

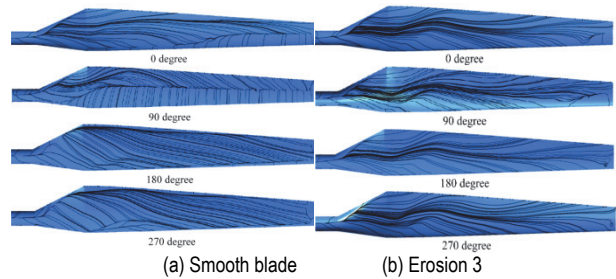


Figure 6 Blade surface limiting streamlines at different azimuth angles under 10 ms<sup>-1</sup> inflow speed

Fig. 6 exhibits significant differences of the surface limiting streamlines between the smooth blade and the leading edge eroded blade. For the smooth blade, when the azimuth angle is 0, most part of the blade gets covered with spanwise separated flow, and only half of the blade is the attached flow. For the eroded blade, only a very small part of the leading edge of the outboard of the blade is covered with the attached flow, indicating that erosion at the leading edge leads to the increase in the flow separation of the blade. When the blade rotates to the position of 90°, the leading edge of the entire smooth blade gets covered with attached flow; however, just about 1/5 area near the blade tip of the delaminated blade does not generate flow separation. When the blade rotates at the higher position (180°), the attached flow disappears gradually, and most part of the blade surface gets covered with the spanwise flow. Only a tiny area of attached flow can be observed at the leading edge near the blade tip of the smooth blade, in contrast, no attached flow can be perceived for eroded blade. When the blade rotates to the highest position (270°), flow separation can be observed both for the entire smooth blade and eroded blade, which is due to the higher wind speed and stall phenomena at this azimuth angle. The results indicate that leading edge erosion can increase the flow separation of the turbine blade and the effect is, in particular, serious at the tip of blade. Notably, more than 70% of the power generation depends on blade tip, thus leading edge erosion significantly influences the aerodynamics of wind turbine. When the inflow velocity

becomes  $20 \text{ ms}^{-1}$  (Fig. 7), the separated spanwise flow can be found both on the smooth and eroded blade at all positions, and no differences in the surface streamlines can be detected between the smooth and eroded blades. Therefore, it can be concluded that leading edge erosion and wind shear significantly influence the surface streamlines at lower wind speed, and exhibit a relatively small influence at higher wind speed.

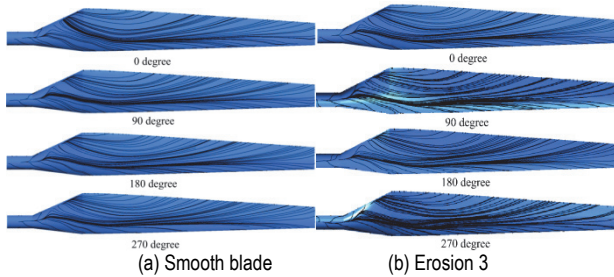


Figure 7 Blade surface streamlines at different azimuth angles under  $20 \text{ ms}^{-1}$  inflow speed

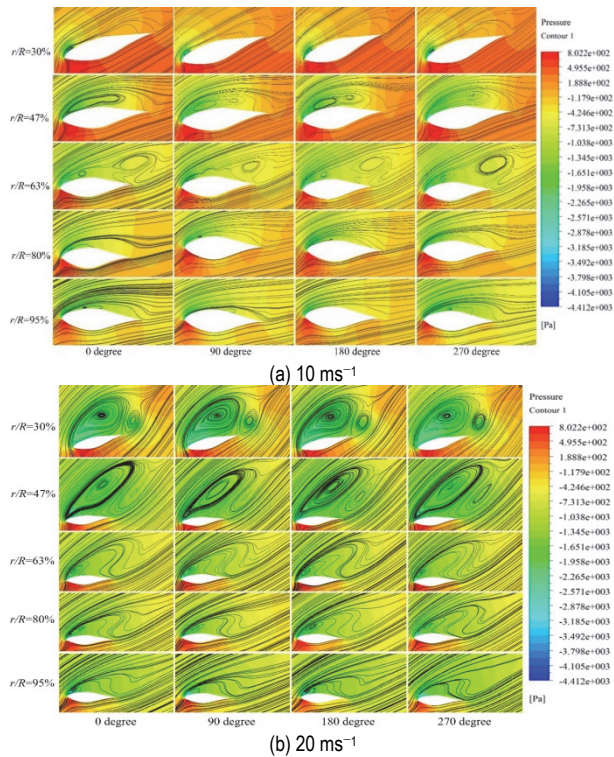


Figure 8 Flow structures around the eroded blade at various azimuth angles

Fig. 8 illustrates the flow structures around the cross sections of the eroded blade at various azimuth angles. The case of Erosion 3 is considered for analysis. Clearly, a small leading edge separation bubble with a length of  $15\%c$  can be detected at the suction surface of the blade at the position  $r/R = 0.3$  for all the azimuth angles. This may be attributed to high angles of attack for the inner side of the blade. When the airflow moves to the stagnation point of the cross section and flows around the leading edge, the raised edge of the delaminated blade prevents the flow and causes separation, finally forming the leading edge bubble. For cross section  $r/R = 0.47$ , the leading edge separation bubble grows bigger and spans almost to the rear surface of the section, which induces a small vortex in the separation area. This may be attributed to the fact that when the mainstream flows over the leading edge and detours the

sharp edge of the delamination at a higher rotating speed and bigger angle of attack, it generates flow separation behind the delaminated area. The separation area keeps growing bigger and turns into a larger vortex at the cross section  $r/R = 0.63$ , where the size of the separation zone is the largest of the entire blade. With the cross section going to the blade tip, the size of the separation region decreases gradually for a smaller angle of attack near the tip.

From the perspective of considering the effects of shear wind on the flow structure around the blade, it can be found that the flow structures are similar when the blade rotates to the azimuth angles of  $0^\circ$  and  $180^\circ$ . However, the separation area is a little smaller at the  $180^\circ$  angle, which may be caused by the blade geometry. When the azimuth angle is  $270^\circ$ , the wind speed is the highest, the entire blade is in stall and the separation is stronger than any other position for an inflow velocity of  $10 \text{ ms}^{-1}$ . The entire blade is in deep stall and the flow separation is stronger at all azimuth angles when the inflow wind speed is  $20 \text{ ms}^{-1}$ ; however, similar to that at the inflow speed of  $10 \text{ ms}^{-1}$ , the flow separation area is a little smaller at the  $90^\circ$  position. Moreover, the separation bubble is almost a circle at sections near the blade root and induces a smaller vortex behind it. For the three sections near the blade tip, only one separation vortex can be observed at the suction surface and the separation area decreases slowly when the section goes to the blade tip.

### 3.2 Impacts on the Pressure Coefficients of the Blade

Fig. 9 illustrates the pressure coefficients of cross sections  $r/R = 0.3, 0.47, 0.63, 0.8, \text{ and } 0.95$  for the blade with various levels of leading edge erosion. It shows that the pressure coefficients of the smooth blade are in accordance with those of the eroded blades at the chordwise position of  $0.4c$  to  $1.0c$ .

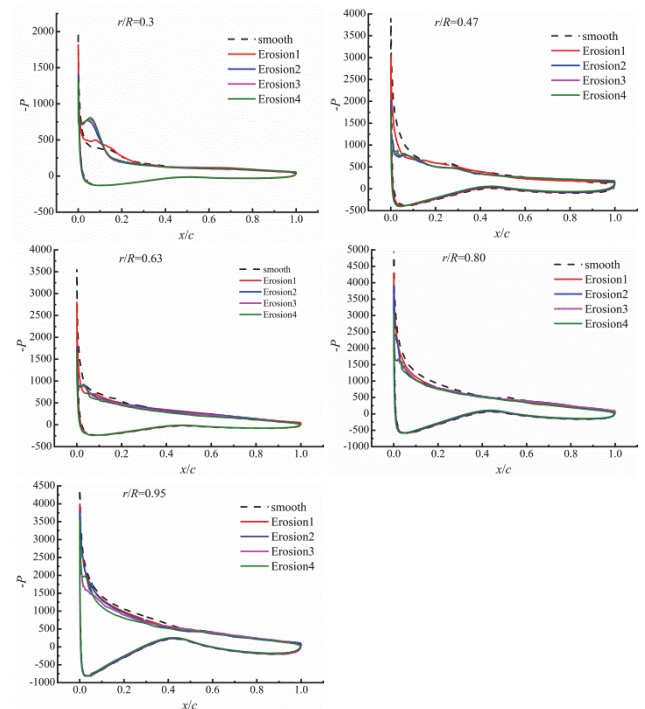


Figure 9 Effects of leading edge erosion on the pressure coefficients at the azimuth angles of  $0$  degree

However, significant deviations can be found at the leading edge of all investigated blades, in particular, at the range of 0.0 to 0.2*c*. For cross section *r/R* = 0.3, the coefficients of the delaminated blades are almost the same, while they exhibit differences from that of the smooth and pitting erosion blades. This may be attributed to the flow separation and deep stall near the root, and leading edge delamination is perhaps beneficial to decrease flow separation, making the pressure difference bigger around the leading edge. However, for sections *r/R* = 0.47, 0.63, 0.80, and 0.95, the pressure coefficient of the smooth blade is the highest, and with the increase in the leading edge erosion levels, the pressure difference between the upper and lower surface declines. This demonstrates that leading edge erosion exhibits notable impact on the aerodynamic performance of the wind turbine; and with the increase in the erosion levels, the aerodynamic performance of the blade decreases.

In order to further explore the influence of shear inflow on the pressure coefficients of leading edge eroded wind turbine, the case of Erosion 3 was selected to study the change rules of pressure coefficients with the azimuth angle, and the corresponding results are shown in Fig. 10.

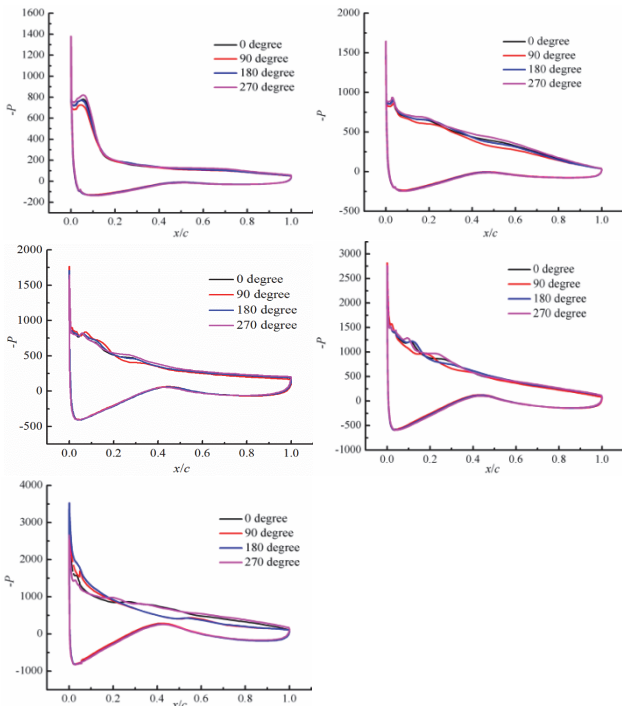


Figure 10 Changes of the eroded blade pressure coefficients at various azimuth angles at 10 ms<sup>-1</sup> wind speed

It shows that the blade has the biggest and the smallest pressure difference between the upper surface and lower surface when the azimuth angles are 270° and 90°, respectively. Moreover, the pressure coefficients are almost similar to each other at the azimuth angles of 0° and 180°. This is due to the effects of the shear action of soil surface, and thus a difference on wind speed is generated at different positions of blade. This is, in particular, notable for blade tip when the blade rotates to the highest and the lowest position. Thus, the pressure difference grows with the sections from blade root to tip.

### 3.3 Effects on Aerodynamic Forces of the Blade

Under shear inflow, the wind speed distributed along the vertical direction is non-uniform, thus we considered not only the inflow direction thrust and torque acting on the wind turbine, but also forces and torques from other directions. The thrust and torque coefficients of the wind turbine in *x*, *y*, and *z* directions are defined in terms of Eqs. (3) and (4):

$$(C_{F_x}, C_{F_y}, C_{F_z}) = \frac{(F_x, F_y, F_z)}{\frac{1}{2} \rho A U_{hub}^2} \tag{3}$$

$$(C_{M_x}, C_{M_y}, C_{M_z}) = \frac{(M_x, M_y, M_z)}{\frac{1}{2} \rho A U_{hub}^2 R} \tag{4}$$

where  $\rho$  is the air density;  $U_{hub}$  is the average wind speed at the hubheight;  $F_x, F_y, F_z$  are the forces exerted on the rotor along *x*, *y*, and *z* direction, respectively;  $M_x, M_y, M_z$  are the torques along *x*, *y*, and *z* direction, respectively;  $\rho$  is the density of the airflow;  $A$  is swept area of the wind rotor; and  $U_{hub}$  is the average velocity at the hub height. The *y* direction is consistent with the axial direction of the wind turbine.

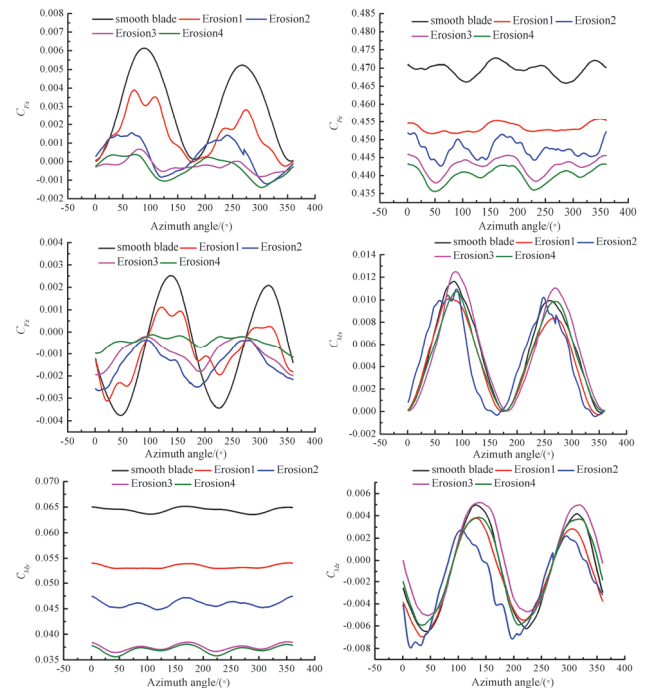


Figure 11 Changes of blade aerodynamic force at various azimuth angles at the inflow speed of 10 ms<sup>-1</sup>

Fig. 11 demonstrates that the thrust and torque coefficients of the wind turbine vary with the azimuth change, and they experience two cycles when the rotor rotates for one week for the turbine composed of two blades. With the increase in the levels of leading edge erosion, the forces exerted on the wind rotor in both *x* and *y* directions decrease, indicating that the thrust exerted on the wind turbine decreases with the increase of the leading edge erosion. When the wind turbine rotates for one week at the inflow speed of 10 ms<sup>-1</sup>, leading edge erosion can

cause an average decrease of 4.0, 5.3, 6.4, and 7.6% of the thrust coefficients  $C_{Fy}$  for Erosion 1, Erosion 2, Erosion 3, and Erosion 4 cases, respectively, when compared with smooth blade. The corresponding decrease of the  $C_{My}$  for the leading edge erosion cases is 19.75, 29.01, 41.82, and 42.54%, respectively. The decrease of  $C_{Fx}$  and  $C_{Fz}$  is smaller than that of  $C_{Fy}$ ; however, all present the declining trend with the increase of leading edge erosion. Nonetheless, the torque coefficients  $M_x$  and  $M_z$  are close to those of the smooth blade, and the differences among all cases are small.

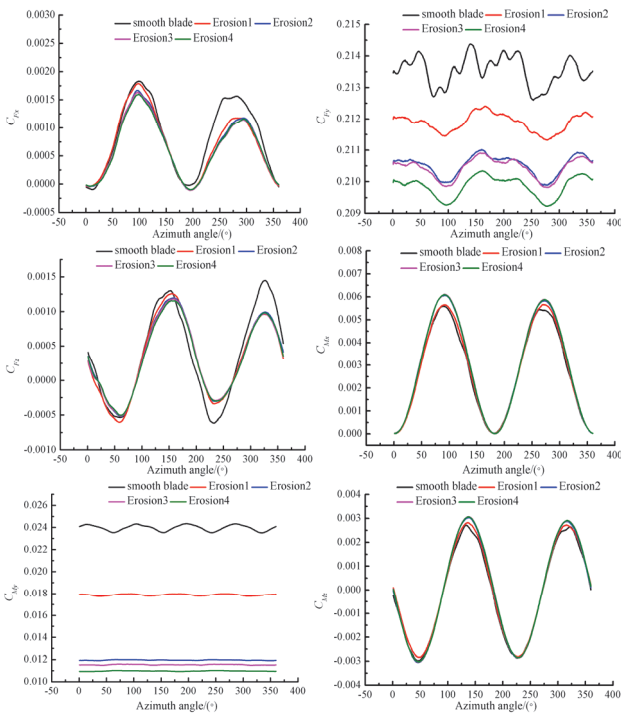


Figure 12 Changes of blade aerodynamic force at various azimuth angles at the inflow speed of 20 ms<sup>-1</sup>

When the inflow velocity increases to 20 ms<sup>-1</sup> (Fig. 12), the decreases of  $C_{Fy}$  caused by leading edge erosion are 0.70, 1.36, 1.40, and 1.85%, respectively, when compared with the smooth blade for the four leading edge erosion cases. Moreover, the decreases of  $C_{My}$  are 25.0, 49.6, 51.3, and 54.6%, respectively. Comparative analysis of the thrust and torque coefficients  $C_{Fy}$  and  $C_{My}$  under 20 and 10ms<sup>-1</sup> inflow velocity indicates that the thrust coefficients decrease at the same erosion level while the torque coefficients increase. It demonstrates that leading edge erosion can lead to more power loss at higher wind speed. However, the differences among all erosion cases are small at 20 ms<sup>-1</sup> wind speed for the deep stall and flow separation, this can also be validated by the surface limiting lines and the flows around the blade in Figs. 7 and 8.

#### 4 CONCLUSIONS

In this study, a numerical study on the effects of the leading edge pitting and three levels of delamination on aerodynamic performance and flow characteristics of NREL Phase VI rotor were conducted under shear inflow. The computation study was carried out with ANSYS-Fluent, and the validation was made by comparing with previous wind tunnel experiment results of smooth blade

[31]. The effects of leading edge erosion on surface limiting streamlines, flow structures around the blade sections, pressure coefficients, and aerodynamic forces were investigated. The main conclusions are as follows:

(a) Significant difference of surface streamlines can be observed between the smooth blade and leading edge eroded blade at the wind speed of 10ms<sup>-1</sup>. The entire blade and more than half of the blade were spanned over the attached flow, while just a tiny area of attached flow could be observed for the eroded blade when the blade was at lower position. When the wind turbine operated at high wind speed, the surface streamlines between the smooth blade and eroded blade were nearly the same.

(b) For the eroded leading edge, small separation bubble could be observed at the suction surface of the section near the blade root. This separation bubble grows bigger and induces a second vortex when the section moves to the middle of the blade. Then, the size of the separation zone gets smaller near the blade tip. The size of the separation region is the smallest when the blade rotates to the lowest position, and in contrast is the biggest at the highest position.

(c) The pressure contribution of the sections for the eroded blade is close to that of the smooth blade at the chordwise position of 0.4c and 1.0c. In contrast, significant deviations occur around the range of 0.0-0.2c of the cross section. With the increase in the erosion levels, the pressure difference between the upper and lower surface decreases, and finally affects the aerodynamic performance of the wind turbine. The pressure difference also varies with the azimuth angle of the blade, which is bigger at the highest position.

(d) Leading edge erosion can cause an average decrease in thrust coefficients reaching up to 7.6 and 1.85% with the rotor rotating for a week at the shear inflow of 10 and 20 ms<sup>-1</sup>, respectively. The torque coefficients decrease by 19.75, 29.01, 41.82, and 42.54% for various leading edge erosion cases at the inflow velocity of 10 ms<sup>-1</sup>; and 25.0, 49.6, 51.3, and 54.6% for the inflow speed of 20 ms<sup>-1</sup>.

These results can aid in the aerodynamic performance prediction of wind turbine operating at environments with sand and salt, where the blade gets easily eroded. However, the shape of the leading edge eroded blade is very complex and difficult to quantify in practical cases, the meshes generation and calculation need great computing resources. In this study, just several simplified geometrical models were adopted, and some initial results were obtained on the impacts of leading edge pitting and delamination on the aerodynamic characteristics of wind turbine under shear inflow. Undeniably, a lot more systematic explorations are still demanded to further investigate the mechanisms and more precise simulations, which will be pursued in the future.

#### Acknowledgements

The authors greatly acknowledge the financial support from the National Natural Science Foundation of China (Grant No. 11902131) and the Natural Science Foundation of Gansu Province (Grant No. 20JR5RA443). The authors are also thankful to D. Simms and coworkers from National Renewable Energy Laboratory for the details and data of the previous study, Ruifeng Hu from Lanzhou University,

and Xuyao Zhang from Lanzhou Jiaotong University for the help in current simulation.

## 5 REFERENCES

- [1] IEA Publications. (2020). World Energy Investment 2020. 5. *International Energy Agency*.
- [2] GWEC Report. (2021). Global Wind Report 2021. *Global Wind Energy Council*.
- [3] Wiser, R. & Bolinger, M. (2018). *Wind Technologies Market Report*. U.S. Department of Energy: Office of Energy Efficiency and Renewable Energy.
- [4] Keegan, M. H., Nash, D., & Stack, M. (2013). On erosion issues associated with the leading edge of wind turbine blades. *Journal of Physics D: Applied Physics*, 46(38), 383001. <https://doi.org/10.1088/0022-3727/46/38/383001>
- [5] Herring, R., Dyer, K., Martin, F. et al. (2019). The increasing importance of leading edge erosion and a review of existing protection solutions. *Renewable and Sustainable Energy Reviews*, 115, 109382. <https://doi.org/10.1016/j.rser.2019.109382>
- [6] Barthelmie, R. J., Shepherd, T. J., Aird, J. A. et al. (2020). Power and wind shear implications of large wind turbine scenarios in the US central plains. *Energies*, 13(16), 4269. <https://doi.org/10.3390/en13164269>
- [7] AWEA. (2020). *Wind Powers America*. 2019 Annual Report. American Wind Energy Association: Washington.
- [8] Li, Z. Y., Wang, X., Huang, G. H. et al. (2020). Ripple analysis and suppression method research of direct drive permanent magnet synchronous wind turbine under wind shear. *Energies*, 13(19), 5088. <https://doi.org/10.3390/en13195088>
- [9] Fernando, H. J. S., Mann, J., Palma, J. M. L. M. et al. (2018). The perdigo: peering into microscale details of mountain winds. *Bulletin of the American Meteorological Society*, 100(5), 799-819. <https://doi.org/10.1175/BAMS-D-170227.1>
- [10] Mahrt, L., Richardson, S., Stauffer, D. et al. (2015). Nocturnal wind-directional shear in complex terrain. *Quarterly Journal of the Royal Meteorological Society*, 140(685), 2393-2400. <https://doi.org/10.1002/qj.2369>
- [11] Albers, A., Jakobi, T., Rohden, R., et al. (2007). Influence of meteorological variables on measured wind turbine power curves. *European Wind Energy Conference and Exhibition 2007*.
- [12] Antoniou, I., Pedersen, S. M., & Enevoldsen, P. B. (2009). Wind Shear and Uncertainties in Power Curve Measurement and Wind Resources. *Wind Engineering*, 33, 449-468. <https://doi.org/10.1260/030952409790291208>
- [13] Walter, K., Weiss, C. C., Swift, A. H. et al. Speed and Direction Shear in the Stable Nocturnal Boundary Layer. *Journal of Solar Energy Engineering*, 131(1), 284-289. <https://doi.org/10.1115/1.3035818>
- [14] Murphy, P., Lundquist, J. K., & Fleming, P. (2020). How wind speed shear and directional veer affect the power production of a megawatt-scale operational wind turbine. *Wind Energy Science*, 5(3), 1169-1190. <https://doi.org/10.5194/wes-2019-86>
- [15] Fadaeinedjad, R., Moschopoulos, G., & Moallem, M. (2009). The impact of tower shadow, yaw error, and wind shears on power quality in a wind-diesel system. *IEEE Transactions on Energy Conversion*, 24(1), 102-111. <https://doi.org/10.1109/TEC.2008.2008941>
- [16] Pedersen, T. F. (2004). On wind turbine power performance measurements at inclined airflow. *Wind Energy*, 7, 163-176. <https://doi.org/10.1002/we.112>
- [17] Papi, F., Cappugi, L., Perez-Becker, S. et al. (2020). Numerical modeling of the effects of leading-edge erosion and trailing-edge damage on wind turbine loads and performance. *Journal of Engineering for Gas Turbines and Power*, 142(11), 111005. <https://doi.org/10.1115/1.4048451>
- [18] Ge, M. W., Zhang, H., Wu, Y. et al. (2019). Effects of leading edge defects on aerodynamic performance of the S809 airfoil. *Energy Conversion & Management*, 195, 466-479. <https://doi.org/10.1016/j.enconman.2019.05.026>
- [19] Rempel, L. (2012). Rotor blade leading edge erosion-real life experiences. *Wind Systems Magazine*.
- [20] Sareen, A., Sapre, C. A., & Selig, M. S. (2015). Effects of leading edge erosion on wind turbine blade performance. *Wind Energy*, 17(10), 1531-1542. <https://doi.org/10.1002/we.1649>
- [21] Offshore Wind Innovation Hub (2018). *Innovation roadmaps*. Glasgow: Offshore Wind Innovation Hub.
- [22] Powell, S. (2011). *3M wind blade protection coating W4600*. Industrial Marketing Presentation.
- [23] Gaudern, N. (2014). A practical study of the aerodynamic impact of wind turbine blade leading edge erosion. *Proceedings of the Journal of Physics: Conference Series, F*. <https://doi.org/10.1088/1742-6596/524/1/012031>
- [24] Gharali, K. & Johnson, D. A. (2012). Numerical modeling of an s809 airfoil under dynamic stall, erosion and high reduced frequencies. *Applied Energy*, 93, 45-52. <https://doi.org/10.1016/j.apenergy.2011.04.037>
- [25] Han, W., Kim, J., & Kim, B. (2017). Effects of contamination and erosion at the leading edge of blade tip airfoils on the annual energy production of wind turbines. *Renewable Energy*, 115, 817-823. <https://doi.org/10.1016/j.renene.2017.09.002>
- [26] Wang, Y., Zheng, X. J., Hu, R. F. et al. (2016). Effects of leading edge defect on the aerodynamic and flow characteristics of an S809 airfoil. *Plos One*, 11(9), 0163443. <https://doi.org/10.1371/journal.pone.0163443>
- [27] Wang, Y., Hu, R. F. & Zheng, X. J. (2017). Aerodynamic analysis of an airfoil with leading edge pitting erosion. *Journal of Solar Energy Engineering-Transactions of the ASME*, 139(14), 061002. <https://doi.org/10.1115/1.4037380>
- [28] Giguere, P. & Selig, M. S. (1999). Design of a tapered and twisted blade for the NREL combined experiment rotor. *NREL/SR-500-26173*. <https://doi.org/10.2172/750919>
- [29] Simms, D., Schreck, S., Hand, M. et al. (2001). NREL unsteady aerodynamics experiment in the NASA-Ames wind tunnel: a comparison of predictions to measurements. *National Renewable Energy Laboratory*. <https://doi.org/10.2172/783409>
- [30] Menter, F. R. (1994). Two-equation eddy-viscosity turbulence models for engineering applications. *AIAA Journal*, 32(8), 1598-1605. <https://doi.org/10.2514/3.12149>
- [31] Mo, J. O. & Lee, Y. H. (2012). CFD Investigation on the aerodynamic characteristics of a small-sized wind turbine of NREL PHASE VI operating with a stall-regulated method. *Journal of Mechanical Science and Technology*, 26(1), 81-92. <https://doi.org/10.1007/s12206-011-1014-7>

### Contact information:

**Yan WANG**, Doctor, Associate Professor  
(Corresponding author)  
a) School of Energy & Power Engineering,  
Lanzhou University of Technology, Lanzhou 730050, China  
b) College of Civil Engineering and Mechanics,  
Lanzhou University, Lanzhou 730000, China  
c) Key Laboratory of Fluid Machinery and Systems of Gansu Province,  
Lanzhou 730050, China  
E-mail: wangyan2008@lut.edu.cn

**Yongfen CHAI**, Graduate Student  
a) School of Energy & Power Engineering,  
Lanzhou University of Technology, Lanzhou 730050, China  
b) Key Laboratory of Fluid Machinery and Systems of Gansu Province,  
Lanzhou 730050, China

**Chenglin DUAN**, Graduate Student

a) School of Energy & Power Engineering,

Lanzhou University of Technology, Lanzhou 730050, China

b) Key Laboratory of Fluid Machinery and Systems of Gansu Province,

Lanzhou 730050, China

**Jian ZHENG**, Doctor, Associate Professor

School of Energy & Power Engineering,

Lanzhou University of Technology,

Lanzhou 730050, China